Steady-state photocarrier grating technique for the minority-carrier characterisation of thin-film semiconductors

2010 J. Phys.: Conf. Ser. 253 012081

(http://iopscience.iop.org/1742-6596/253/1/012081)

Journal of Physics: Conference Series **253** (2010) 012081 doi:10.1088/1742-6596/253/1/012081

Steady-state photocarrier grating technique for the minority-carrier characterisation of thin-film semiconductors

R Brüggemann
Institut für Physik, Carl von Ossietzky Universität Oldenburg, 26111 Oldenburg, Germany

E-mail: rudi.brueggemann@uni-oldenburg.de

Abstract. The steady-state photocarrier grating technique allows the determination of the ambipolar diffusion length in low-mobility semiconductors and provides access to the minority-carrier properties in terms of the mobility-lifetime product. The technique probes the excess carrier distribution under the presence of a sinusoidally modulated photogeneration rate which is achieved by the superposition of two coherent laser beams. The relatively simple technique has been established in many laboratories and has been successfully applied to a variety of thin-film semiconductors. The basic theory of the method, experimental set-ups, variants of the experimental realisation in terms of the grating-period or the electric-field variation and some of the various applications of the steady-state photocarrier grating method on thin-film silicon, chalcopyrite and other semiconductors are presented and reviewed in this contribution. Worthwhile information can be obtained on the recombination and the density-of-states in the band-gap of the semiconductor from experiments with the steady-state photocarrier grating method in combination with dark- and photoconductivity measurements.

1. Introduction

The steady-state mobility-lifetime products of electrons and holes represent the photoelectronic properties of the majority and minority carriers under stationary illumination, in contrast to the mobility-lifetime products from transient photocurrent experiments like time-of-flight. Both mobility and lifetime are important properties which determine transport and recombination. In contrast to the majority-carrier properties which can be determined rather straightforwardly by stationary photocurrent measurements under the assumption that the minority-carrier contribution can be neglected, the minority-carrier properties can only be revealed by more sophisticated methods. In this respect the steady-state photocarrier grating (SSPG) technique has had an enormous impact since it was suggested by Ritter, Zeldov and Weiser named RZW hereafter, in 1986 [1].

RZW outlined in their paper on the diffusion length measurement in photoconductive insulators the basic features of the SSPG technique which is based on the carrier diffusion under the presence of a spatial sinusoidal modulation in the photogeneration rate achieved by the interference of two coherent laser beams – technically achieved by splitting the beam from a laser by a beam splitter. The resulting modulation in the photogeneration rate in the semiconductor bulk induces a so-called photocarrier grating with a spatial modulation in the excess carrier densities. From photocurrent measurements at different grating periods the ambipolar diffusion length can be determined by the RZW analysis that assumes ambipolar transport and charge neutrality.

The proposal by Ritter *et al* [1], following papers on the analysis [2,3] and the relatively simple set-up triggered the wide-spread application of the SSPG method. It was quickly adopted in other laboratories [4-8].

In parallel, critical and more in-depth accounts on the underlying theory were given to put the technique on a firm ground or to describe its limits when applied to semiconductors with traps, in extension to the rather intuitive theoretical approach in the early publication. In a later analysis Ritter *et al* [9] numerically solved the transport equations in the small-signal approximation and confirmed the validity of the approach in the "lifetime regime", in which the dielectric relaxation time under illumination, determined from the relaxation time with photoconductivity, is much shorter than the carrier lifetimes – in contrast to the "relaxation time regime". Theoretical accounts were also given by Balberg [10,11], Li [12], Sauvain *et al* [13], Abel *et al* [14] and Hattori *et al* [15]. The latter authors showed that under the conditions in the "lifetime regime" the RZW evaluation procedure of the SSPG technique gives correct results.

In this article, the SSPG method will be introduced, the experimental measurement procedure will be outlined and details of the data analysis will be described. An overview on the applications of SSPG on a variety of semiconductors will then be given which illustrate that SSPG has become a widespread technique that is established in many laboratories.

2. Description of the SSPG concept

Figure 1 illustrates the beams L_1 and L_2 which represent plane waves with wavelength λ which impinge on the semiconductor where they suffer refraction according to Snell's law so that the angle between the two beams changes from θ to θ'. The analysis of the plane-wave interference for weak absorption in *z* direction results in a photogeneration-rate pattern $G(x,y,z)$ according to [1]

$$G(x,y,z) = G(x) = (G_1 + G_2) + 2\gamma_0 \left(G_1 G_2\right)^{0.5} \cos\left(2\pi x/\Lambda\right) \tag{1}$$

where G_1 and G_2 refer to the photogeneration rate resulting from beam L_1 and L_2 alone. A grating quality factor γ_0 is introduced here with values close to 1 for a good grating quality.

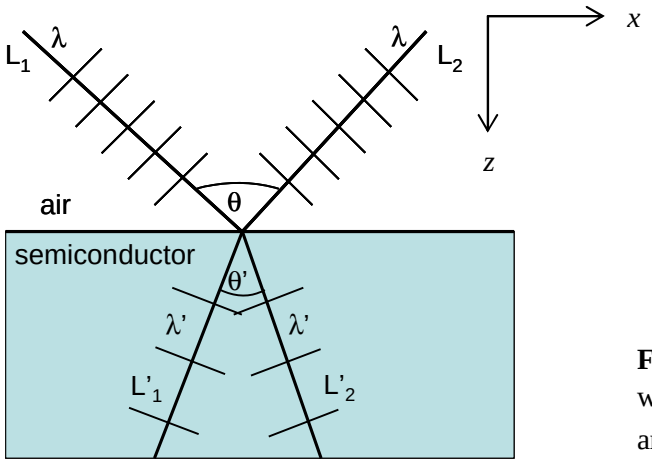

Figure 1. Sketch of the interference experiment with two planes waves from the laser beams L_1 and L_2.

Under the typical conditions with coplanar electrodes on a thin-film semiconductor with a gap in the range of say 0.3 mm to 2 mm, the number of grating periods amounts to a few hundred at typical grating periods in the range of 1 µm.

The grating period in equation (1) is given by

$$\Lambda = \lambda / \left[2\sin\left(\theta/2\right) \right] \tag{2}$$

for which it is noted that it is only the angle θ between the two beams in air that enters the equation. For weak absorption in which the generation rate is almost constant in the *z* direction there is only an *x* dependence in $G(x)$.

The RZW analysis suggests to exploit two conditions of the laser-beam arrangement at a given Λ: one measurement under coherent conditions with current density $j_{\mathrm{coh}}(\Lambda, L_1 + L_2)$ and one measurement under incoherent conditions with current density $j_{\mathrm{inc}}(\Lambda, L_1 + L_2)$. RZW also suggested that a lock-in technique may be used with relative measurement to the current density with one beam only, with $j_1(\Lambda, L_1)$. A parameter $\beta(\Lambda)$ is defined given by

$$\beta(\Lambda) = \frac{j_{\mathrm{coh}}(\Lambda, L_1 + L_2) - j_1(\Lambda, L_1)}{j_{\mathrm{inc}}(\Lambda, L_1 + L_2) - j_1(\Lambda, L_1)} = \frac{U_{\mathrm{coh}}(\Lambda)}{U_{\mathrm{inc}}(\Lambda)}, \tag{3}$$

where $U_{\mathrm{coh}}(\Lambda)$ and $U_{\mathrm{inc}}(\Lambda)$ are lock-in amplifier measurements under coherent and incoherent conditions. For a number of position that relate to different grating periods Λ, the parameter $\beta(\Lambda)$ is determined by measuring $U_{\mathrm{coh}}(\Lambda)$ and $U_{\mathrm{inc}}(\Lambda)$.

RZW related this $\beta(\Lambda)$ parameter with the ambipolar diffusion length *L* according to

$$\beta\left(\Lambda\right) = 1 - \frac{2Z}{\left[1 + \left(2\pi L / \Lambda\right)^2 \right]^2} \tag{4}$$

From a measured set of β values at a number of Λ positions a fit can be made with the two fit parameters *L* and *Z*. While L is the diffusion length that one wants to determine Z is a fit parameter, typically between 0.5 and 1, which contains information on the grating quality, the intensity dependence of the photoconductivity and the ratio between dark and total current under illumination [1].

Equation (4) can be changed to a form

$$\left(1-\beta\right)^{-1/2} = \left[\left(2Z\right)^{-1/2} \left(1/L\right)^2 \right] \left(2\pi/\Lambda\right)^2 + \left(2Z\right)^{-1/2}, \quad \begin{matrix} L = \left(\dfrac{a}{b} \right)^{1/2} \\ Z = (2b^2)^{-1} \end{matrix} \tag{5}$$

in which measured β values are processed to be plotted as ordinate values or alternatively to [7

$$1/\Lambda^2 = \left[Z^{1/2} / \left(2\pi L\right)^2 \right] \left[2/\left(1-\beta\right) \right]^{1/2} - \left(2\pi L\right)^{-2}, \quad \begin{matrix} L = \left(\dfrac{1}{-4\pi^2 b} \right)^{1/2} \\ Z = \dfrac{a^2}{b^2} \end{matrix} . \tag{6}$$

Here, *L* and *Z* are determined from linear fits.

The relation to the minority-carrier properties can be shown to be given by [14]

$$L = \sqrt{2\frac{e}{kT}\frac{(\mu\tau)_{\min}(\mu\tau)_{\mathrm{maj}}}{(\mu\tau)_{\min}+(\mu\tau)_{\mathrm{maj}}}}\,, \tag{7}$$

where the minority carrier mobility-lifetime $(\mu\tau)_{\min}$ product is determined by the product of the free carrier mobilities $\mu_{\min}$ and the free carrier recombination lifetime $\tau_{\min}$. For the majority carriers holds, $(\mu\tau)_{\mathrm{maj}} = \mu_{\mathrm{maj}}\tau_{\mathrm{maj}}$.

Complementary, the steady-state photoconductivity σ_{ph} is given by

$$\sigma_{\mathrm{ph}} = eG\left[(\mu\tau)_{\min}+(\mu\tau)_{\mathrm{maj}}\right]. \tag{8}$$

These two equations with the two unknowns allow the $(\mu\tau)_{\mathrm{maj}}$ and $(\mu\tau)_{\min}$ determination but no straightforward correlation on whether the electrons or the holes are the majority/minority carriers. In the typical case that one carrier type dominates the two equations (7) and (8) reduce to

$$L = \sqrt{2\frac{e}{kT}(\mu\tau)_{\min}}\,, \tag{9}$$

and

$$\sigma_{\mathrm{ph}} = eG(\mu\tau)_{\mathrm{maj}}\,. \tag{10}$$

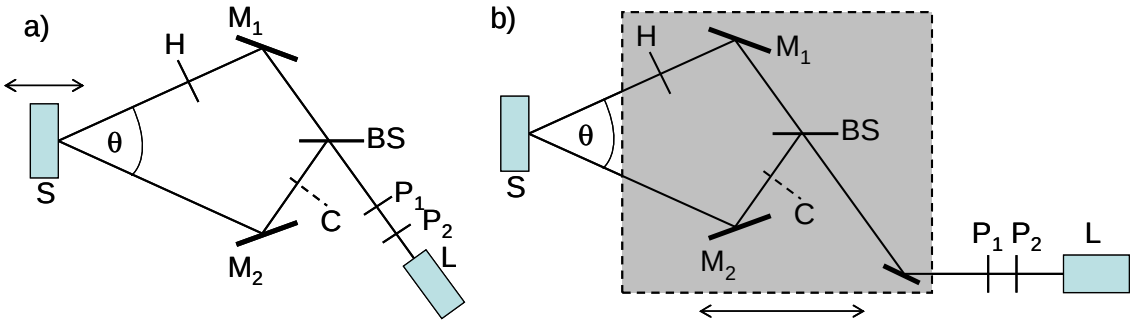

Figure 2. Schematic of the experimental setups that may be used for the SSPG method. The double arrow indicates which element is moved linearly in order to change the angle between the two beams that originate from one laser beam of a laser L that is split by a beam splitter (BS). In (a) the sample S is moved; in (b) an optical table, indicated by the shaded area, is moved. Such a set-up has been arranged by C. Longeaud and R. Brüggemann at LGEP, Paris. H denotes a half-wave plate and C a chopper. P1 and P2 are polarisation filters, M1 and M2 are mirrors.

3. Experimental set-up

A variety of experimental set-ups is possible for the SSPG technique. A common feature is the splitting of a laser beam which is then guided symmetrically onto the sample in order to induce an interference grating. For example, the two beams from the laser L, split by the beam splitter BS, hit the sample S in the gap between the electrodes in figure 2(a) which is drawn according to the original proposal by RZW. The sample is moved on a linear stage to change the angle between the two beams. The beam splitter BS separates the photon flux of the two beams such that the ratio is in the range of

10 or less. The half-wave retardation plate H is positioned in the strong beam, in order to rotate the polarisation, i.e., rotation of H by 45° changes the polarisation of the beam by 90°. An additional feature, not contained in [1] are the polarisation filters which define the polarisation and can also be used for a variation of the photon flux by rotation of the polarizer P2, keeping P1 fixed.

Figure 2(b) is different in that most of the optical elements are arranged on an optical table that is moved along a linear stage. The sample S is fixed. The advantage here is that the length of the light path is the same for every grating period while in arrangement (a) the length of the path changes and the laser spot may widen at longer distances. Depending on the cryostat that is available for temperature-dependent measurements, the arrangement in (b) can work with a fixed cryostat while in (a) the cryostat must be flexible enough to be moved over distances in the range of typically at least 1 meter.

4. Results

This chapter discusses results on the photoconductive properties on a number of thin-film semiconductors like hydrogenated amorphous silicon and its alloys in relation to the SSPG method, i.e., the minority-carrier properties in the steady state. As these are linked with the majority-carrier properties the latter will also be discussed in comparison when appropriate.

4.1. Hydrogenated amorphous silicon

Hydrogenated amorphous silicon (a-Si:H) has been in the focus of SSPG applications since the early work by Ritter *et al* [1] in which the method was demonstrated on a-Si:H. Figure 3 shows typical experimental data from our laboratory of a device quality a-Si:H in a β vs. Λ plot (a) (equation 4) and in a linear plot (b) (equation 5). The very good agreement between the two evaluation schemes with L = 154 nm indicates the quality of the measurements.

Figure 4 shows SSPG results for a high-defect a-Si:H sample. In contrast to the previous figure the β values are almost constant. Note also that the variation in the ordinate values in figure 4(b) is much less than in figure 3(b). The good agreement between the two evaluations is a good indicator that the measurement is reliable even though the diffusion length is short.

It is noted that it is not possible to achieve such a good agreement for all samples under all the different conditions like low temperature or low generation rate. Any deviations between the values of the two analyses can be inspected and in some cases exempting individual data points may results in better agreement. The experimental error in the linear plot may become larger for larger β because of the 1 - β term in the denominator in equations (5) or (6).

4.1.1. Temperature and generation-rate dependence. In figure 5(a), the experimentally determined monotonous decrease of $(\mu\tau)_p$ with decreasing temperature is a signature often exhibited by a-Si:H samples. The experimental results in figure 5(a) can be roughly reproduced by numerical simulation of the photoelectronic properties of a-Si:H in figure 5(b) [16,17]. The increase in the splitting of the quasi-Fermi levels with decreasing temperature is related to an increase in the density of effective recombination centres for the excess carriers. These typically recombine through the electronic states between the quasi-Fermi levels leading to the observed decrease in lifetime or $(\mu\tau)_p$ with decreasing temperature.

At a given temperature, the mobility-lifetime products in figure 5 drop with increasing photogeneration rate G which is related to the above-mentioned increase in quasi-Fermi level splitting. There has been some controversy in the literature about the consequences of the G dependence with respect to density-of-states models in the band-gap of a-Si:H. Balberg *et al* [18] suggested that one correlated dangling bond level is not sufficient to explain the experimental data and he suggested that there is evidence for a defect-pool model based defect distribution with more than one defect peak.

The Neuchatel group pointed out that a proper balancing of charge in one correlated dangling bond and in the band-tail states can also explain the experimental findings [13].

4.1.2. Fermi-level position. For *n*-type samples there is a well-known increase in the photoconductivity with increasing dark conductivity. The change of the occupation of dangling bonds becoming negatively charged and thus more ineffective for electron capture, results in the increase in the lifetime despite a possible increase of the absolute dangling bond density upon doping. In terms of mobility-lifetime products, the situation in figure 6(a) has been established [19]. It shows $(\mu\tau)_{\min}$ and $(\mu\tau)_{\mathrm{maj}}$ for quite a number of samples plotted vs. Fermi level position $E_c - E_f$. The whole set of data points illustrates that for *n*-type samples with smaller $E_c - E_f$ the electrons are the majority carriers and here $(\mu\tau)_{\mathrm{maj}} >> (\mu\tau)_{\min}$. The value for $(\mu\tau)_{\mathrm{maj}}$ increases with higher doping until at the highest doping levels the dangling bond density has become too large so that $(\mu\tau)_{\mathrm{maj}}$ then decreases with further shift of E_f towards E_c.

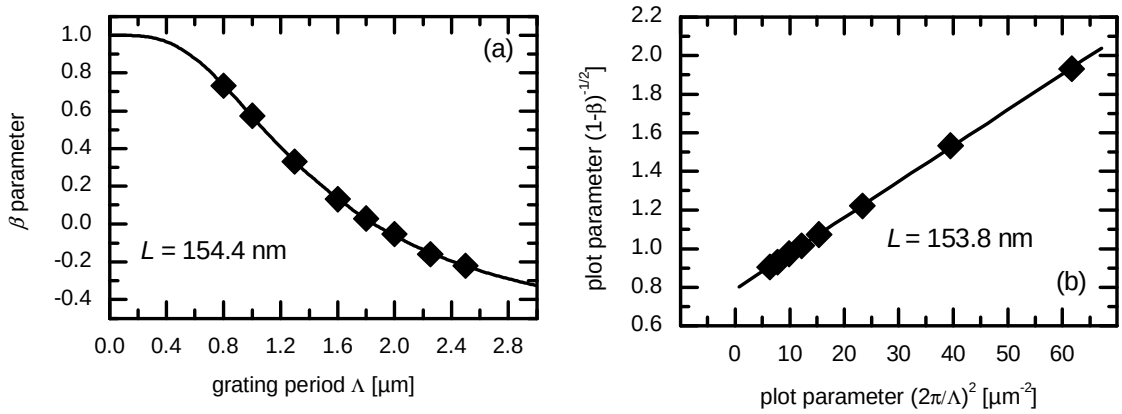

Figure 3. The symbols represent the experimental data points for an undoped a-Si:H sample. The full lines are fits. Both types of analysis give good agreement in the value for *L*.

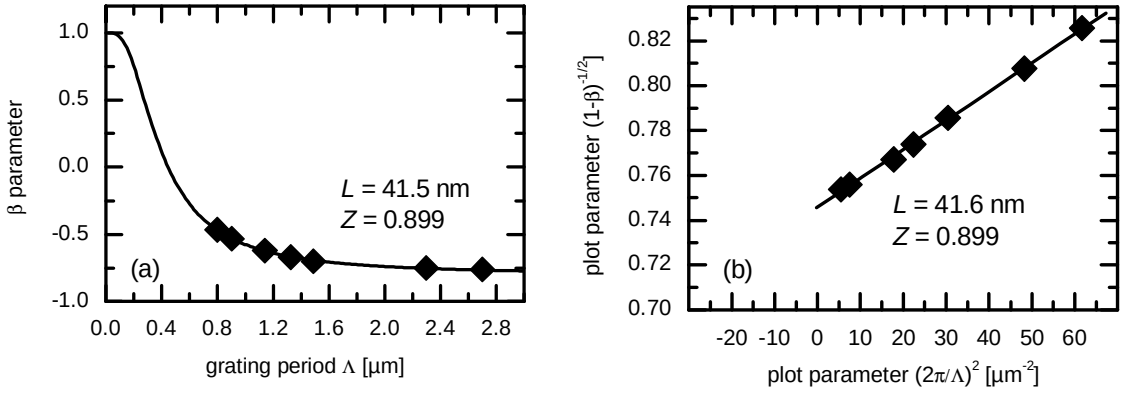

Figure 4. The symbols represent the experimental data points for a high-defect density undoped a-Si:H sample. The full lines are fits. Both types of analysis give good agreement in the value for *L*.

For *p*-type samples the role of the electrons and the holes changes. Here, again $(\mu\tau)_{\mathrm{maj}}$ >> $(\mu\tau)_{\mathrm{min}}$ and $(\mu\tau)_{\mathrm{maj}}$ = $(\mu\tau)_{\mathrm{p}}$. There is no full symmetry in the figure because the underlying density-of-states distribution in the band-gap is not symmetric. The lines are results from numerical simulation with a full model for charge neutrality, with dangling bonds and recombination which reproduces the experimental tendency quite well [19].

The ratio $b=(\mu\tau)_{\mathrm{n}}/(\mu\tau)_{\mathrm{p}}$ in figure 6(b) covers quite a wide range. For most of the nominally undoped samples with $E_{\mathrm{c}}-E_{\mathrm{f}}$ in the range 0.65 eV to 0.75 eV, *b* is in the range of 20 to 300, indicating that electrons are the majority carriers in undoped a-Si:H. The presentation also indicates that there is no one-to-one relation between *b* and $E_{\mathrm{c}}-E_{\mathrm{f}}$ but that the ordinate values show some scatter e.g. for *n*-type samples.

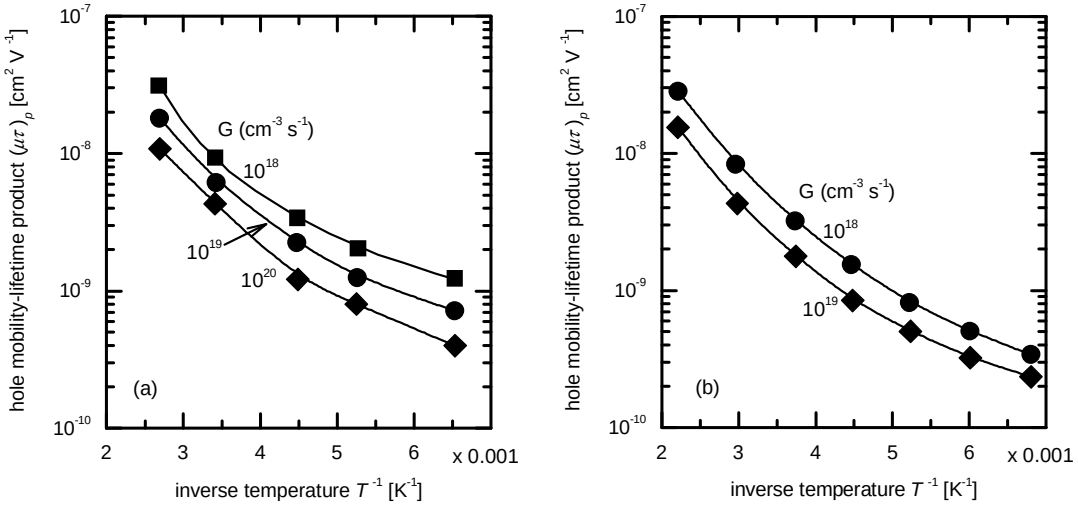

Figure 5. Temperature dependence of the $(\mu\tau)_{\mathrm{p}}$ product of an undoped a-Si:H sample at different photogeneration rates (a), after [17]. Numerical-simulation results with a free-hole mobility of 1 cm^2 V^{-1} s^{-1} which reproduce the monotonous $(\mu\tau)_{\mathrm{p}}$ with decreasing temperature (b), after [18].

Shortly after the SSPG proposal, the properties of intentionally doped films were studied by Yang *et al* [6]. Low-concentration boron doping was shown to lead to an increase in the diffusion length, in agreement with figure 6(a). With higher doping level the diffusion length dropped drastically. These results were interpreted as a change in the minority-carrier type. For the higher doping levels and the shift of the Fermi level towards the valence-band edge, the electrons become the minority carriers and the increasing defect density upon doping then leads to the reduction in the diffusion length. An important observation was a benefit in the diffusion length at small shifts of E_{f} towards mid-gap which was thought to be beneficial for the net *i*-layer carrier collection in a-Si:H based *pin* solar cells.

4.1.3. Electric-field effects. In the early publications on SSPG there has been concern with respect to the electric-field limitations in two ways: electric-field modulation due to space charge and phase shift in the modulation of the electron and hole distributions because the electric field *E* pulls these apart.

The analysis by Abel *et al* [14] takes into account electric-field effects and can been applied to study the β dependence on grating period Λ and electric field E. An example is given in figure 7 [20].

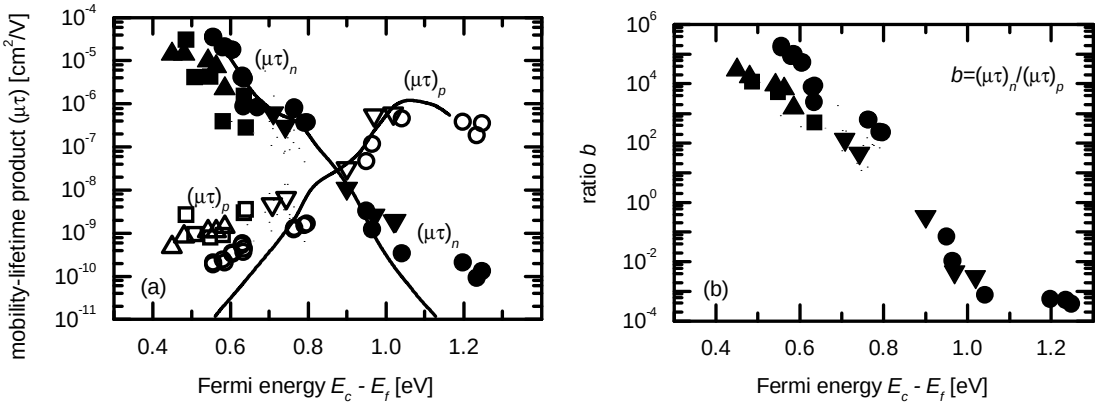

Figure 6. Variation of the mobility-lifetime products (a) and the ratio b (b) for the variation of the Fermi level by doping. Different symbols denote different sample series. The full line is from numerical simulation to model the behaviour of the data represented by the circles, after [19].

Figure 7(a) is a check that the incoherent contributions maintain Ohmic character even at the high voltages, represented by a slope of 1 in the log-log plot. For the coherent contribution there is some deviation so that a voltage-dependent β is the result. The full lines in Figure 7(b) are fits according to the theory by Abel *et al* [14] which includes both the effect of space charge and external electric field. It is noted that, depending on the measurement position, i.e., Λ value, there is quite a variation in the range of the measured β values when the voltage is increased. Good agreement could be achieved between the experiment and the fit functions for the different grating periods. Accounts on the effective dielectric relaxation time could thus be given [20].

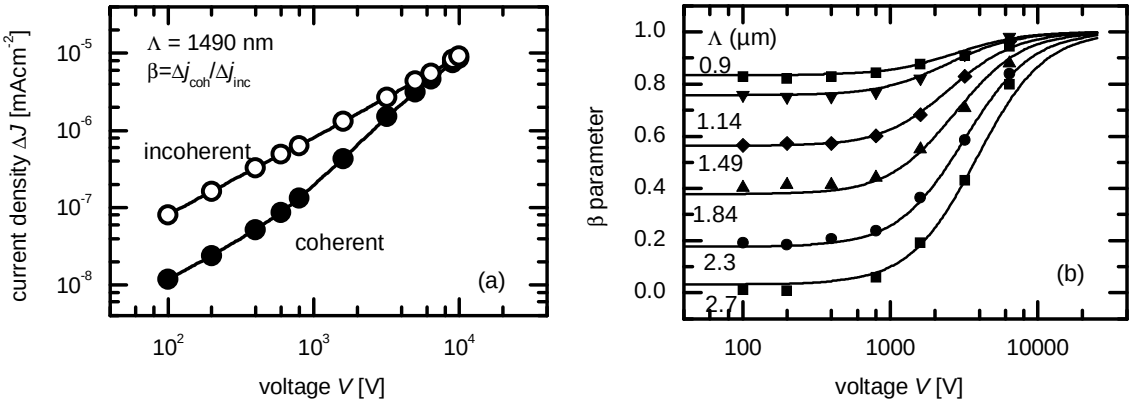

Figure 7. Experimental E dependence of the SSPG data of a sample with electrode gap 0.5 mm. The open symbols in (a) demonstrate the Ohmic character under incoherent conditions. The full data points vary linearly with voltage only up to 8 kV/cm (400 V). In (b), for the coherent case, the drop in photocurrent is no longer maintained at high E. The voltage dependence of β was measured at the different grating periods, indicated in (b), after [20].

4.1.4. Light-soaking and degradation. The time-dependent decrease of the photocurrent is a signature of many a-Si:H films, the details of which are analysed in terms of defect-creation models. Any increase in the defect density should also have an influence on the minority-carrier properties so that SSPG measurements in combination with light-induced degradation may reveal the underlying recombination physics that is determined by the time-dependent increase in the dangling-bond density upon illumination. In view of the Fermi-level related discussion above it is illustrative to point out the possibility that the diffusion length may increase upon light-soaking, as illustrated by the SSPG results in figure 8. The figure shows that for a nominally undoped a-Si:H sample the Fermi level shifted towards mid-gap upon light-soaking leading to an increase in the diffusion length although more defects have been created. Upon the Fermi-level shift, the defects become less negative and thus less attractive for hole capture, so that the minority carrier properties in terms of *L* can be improved.

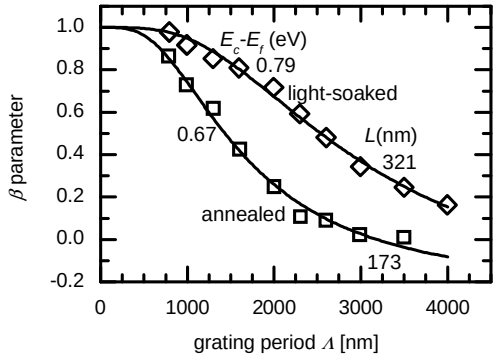

Figure 8. Increase of the diffusion length upon light-soaking of a-Si:H, after [21].

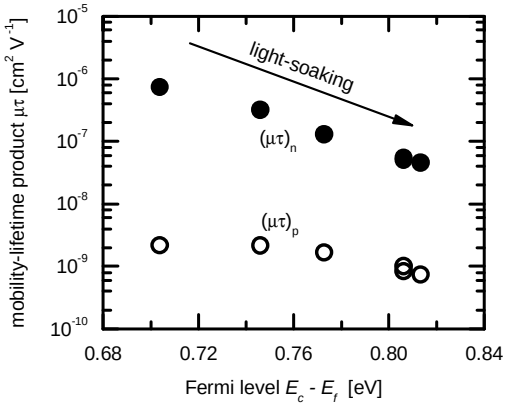

Figure 9. Effect of light-soaking on the Fermi level and the mobility-lifetime products. Compilation after Morgado [22].

With respect to the influence of the mobility-lifetime products on the Fermi level and the reported change of the Fermi level upon light-soaking, it appears very helpful to always monitor the dark current upon degradation. It is then interesting to discuss the light-soaking results by Morgado [22], which are compiled in figure 9. These changes give an indication of new defect creation as the Fermi level shifts but *L* or $(\mu\tau)_p$ does not increase in contrast to figure 8. Upon longer light-soaking both mobility-lifetime products show a decrease which Morgado also related to the variation in the sub-gap absorption and defect density.

The combination of dark current, photocurrent and SSPG measurements has the potential to further elucidate the details of light-induced recombination and may, together with numerical modelling of the experiments, shed light on the question under which condition the main recombination channel is either via dangling bonds or via the band-tails and how and if there is a transition between the two channels by changing the temperature or the photogeneration rate

4.2. Hydrogenated silicon germanium

One of the first reports on the application of the SSPG method was given by Bauer *et al* [4] on hydrogenated amorphous silicon germanium (a-$Si_{1-x}Ge_x$:H) alloys. The focus of this research and later publications on these alloys was to characterise the photoelectronic properties for samples with increasing x and to study the influence of Ge incorporation and its influence on the defect density and the band tails. Typically, both the photoconductivity as a signature of the majority carriers and the diffusion length as a signature of the minority carriers decrease with increasing x but they are affected in a different way by the concomitant shift of the Fermi energy towards mid-gap [23].

Figure 10 summarises the hole mobility-lifetime products for quite a number of a-$Si_{1-x}Ge_x$:H samples as a function of Ge content. For x < 0.43, the values of the $(\mu\tau)_p$ product stay > 10^{-9} cm^2 V^{-1}, i.e., diffusion lengths of about 100 nm. Fölsch *et al* [24] report slightly larger values in this x-range. These authors report a strong drop in $(\mu\tau)_p$ for x larger than 0.5 at which the combination of increasing dark conductivity and decreasing photoconductivity makes the diffusion length very difficult to measure.

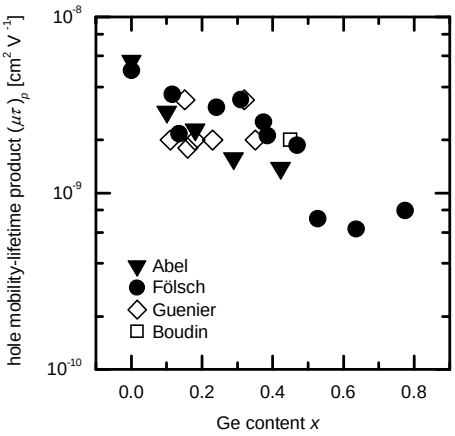

Figure 10. Hole mobility-lifetime products of a- a-$Si_{1-x}Ge_x$:H and pm-$Si_{1-x}Ge_x$:H thin films. Optimised films maintain a diffusion length in the range of 100 nm. At x = 0.45 there is a strong drop in the mobility-lifetime products. More details are in the text.

The data by Gueunier *et al* [25] on so-called polymorphous silicon germanium alloys (pm- $Si_{1-x}Ge_x$:H) are added in figure 10 in the range up to x=0.35 at which the optical gap E_{04}, i.e., the energy at which the absorption coefficient is 10^4 cm^{-1}, was 1.5 eV. The reported *L* values of the annealed samples scatter in the range between 100 nm and 130 nm, values as also reported by Bhaduri *et al* [26] in the range x = 0.4 – 0.5 and represented by the symbol at x = 0.45 in figure 10. The selected results above show that it is possible to deposit hydrogenated amorphous silicon-germanium alloys in a Ge-content range x < 0.45 for which the deterioration in the photoelectronic properties is not too severe.

4.3. Hydrogenated amorphous silicon carbide

The diffusion length from SSPG was determined by Li *et al* [27] for a corresponding characterisation and optimisation of hydrogenated amorphous silicon carbide films (a-$Si_{1-x}C_x$:H) of different band gaps and different feed stock gases. These authors find a correlation between the increase of the diffusion length and better solar cell properties. They make it clear though that, as mentioned above, the sole

value of the diffusion length may not be the only indicator of the defect density of a sample. They deduce from the complementary photo- and dark conductivity results that Fermi level related occupation of defects may have lead to higher values of the diffusion length of some of their a-$Si_{1-x}C_x$:H samples.

Mohring *et al* [16,17] reported on the temperature-dependent and generation-rate dependent mobility-lifetime products of majority- and minority carriers in optimised a-$Si_{1-x}C_x$:H with an optical band gap up to 1.95 eV. For the alloys, the $(\mu\tau)_p$ product decreases with decreasing temperature, similar to the findings in figure 5 for a-Si:H. At any temperature $(\mu\tau)_p$ decreases with increasing x which has been related by Mohring *et al* to the increased dangling bond density with increasing x. For a-$Si_{1-x}C_x$:H with a band gap of 1.94 eV, a value of $(1\text{-}2)\times10^{-9}$ cm^2 V^{-1} for $(\mu\tau)_p$ was determined. and with $(\mu\tau)_n$ about a factor of ten higher.

4.4. Hydrogenated microcrystalline silicon

The terms polycrystalline silicon, because of some large-grain materials, or nanocrystalline silicon, because of the nanocrystallites in a microcrystalline structure, were temporarily fashionable for what is typically subsumed today under hydrogenated microcrystalline silicon (µc-Si:H). The application of the SSPG method to microcrystalline silicon is rather straightforward on the one hand as, for example, sample geometries and absorption coefficients are somewhat but not significantly different. On the other hand, there are some obstacles involved because of the typically higher dark conductivity and some possible effect of surface roughness, which reduces the grating quality.

Droz *et al* [28] expand on the similarity in the transport between amorphous and microcrystalline silicon. Especially, both the majority and minority carrier properties as a function of doping level were shown to be similar to a-Si:H. Goerlitzer *et al* [29], Brüggemann [30] and Okur *et al* [31] report that the fitting parameter *Z* takes small values in µc-Si:H because of the small ratio of photo- to dark conductivity. Another obstacle is the reduction in the grating quality factor because of optical scattering which deteriorates the grating. The *Z* parameter was shown to increase after polishing the rough surface of µc-Si:H samples [30].

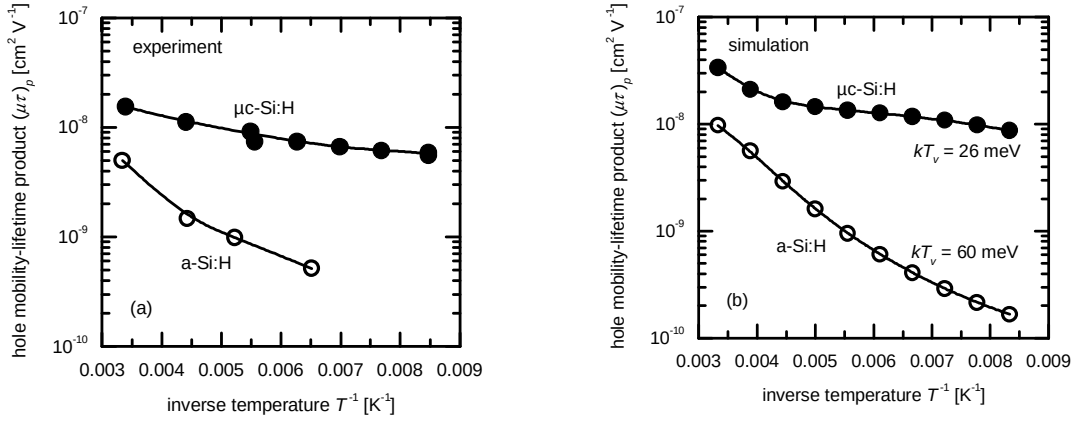

Figure 11. Temperature dependence of the majority and minority carrier mobility-lifetime products of µc-Si:H with a comparison of the experimental (a) and the simulation (b) results, after [32]. The valence-band tail is described by an exponential exp[-*E*/(*kT*$_V$)].

The temperature dependence of $(\mu\tau)_p$ with a nominal crystalline volume fraction from Raman spectra of 0.66 was studied by Brüggemann and Kunz [32], as shown in figure 11. In contrast with a-Si:H, the experimental temperature-dependent decrease of $(\mu\tau)_p$ is much less than in a-Si:H. Application of numerical modelling, with which the small decrease can be reproduced (figure 11(b)) indicates that an introduction of a steeper valence-band tail in the low-band gap µc-Si:H leads to the different behaviour in comparison with a-Si:H.

Balberg [33] also reported on the temperature dependence of the two mobility-lifetime products of µc-Si:H and their dependence on the photogeneration rate. In addition to the experimental data they also performed numerical simulations in order to correlate the experimental and simulation results. Close inspection of this comparison shows that the agreement is not always good. Some of the input parameters in the model for the simulation have rather extreme values so that here is still a challenge here to provide more experimental evidence for this proposed model.

A relation between the diffusion length and the deep defect density was presented by Brüggemann [34]. It was shown that *L* is correlated with the optical absorption coefficient at 0.8 eV. A value of 0.8 eV was chosen in order to represent an energy that is out width a band-tail region and deeper in the band-gap. The experimental data from quite a number of samples are shown in figure 12. The two open symbols represent one µc-Si:H sample in which the deep defect density was increased by proton irradiation [35]. For this sample the increase in the absorption coefficient upon irradiation correlates almost inversely linearly with a decrease in *L*. For the other samples there is substantial scatter. It may thus be possible that for low absorption coefficients another recombination channel limits the minority-carrier lifetime. Similar experiments on relating sub-gap absorption with the diffusion lengths in microcrystalline silicon were reported by Günes *et al* [36].

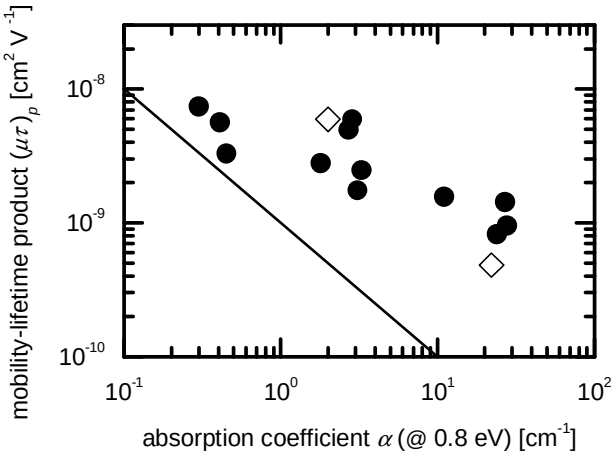

Figure 12. Variation of the room-temperature diffusion length with the absorption coefficient at 0.8 eV of a number of microcrystalline silicon samples, after [34].

There are indications that transport is inhomogeneous in µc-Si:H with respect to the transport path parallel or perpendicular to the film-growth direction. The SSPG experiment with coplanar electrode geometry and transport perpendicularly was complemented by the Prague group with surface-photovoltage (SPV) measurements for the diffusion length determination parallel to the growth direction to which the reader is referred [37]. For the SPV evaluation one must be careful as drift contributions were alleged to result in longer SPV diffusion lengths than determined by SSPG in a-Si:H.

4.5. Hydrogenated microcrystalline germanium

Badran *et al* [38] reported on the determination of the minority-carrier diffusion length in microcrystalline germanium (µc-Ge:H). Because of the high dark conductivity it was necessary to

perform the SSPG experiments at lower temperature for the photocurrent to be measurable. The measured diffusion lengths were quite short. The conclusion by Badran *et al* was that µc-Ge:H appears suitable for diode applications as a sensor, as was demonstrated previously, under reverse bias but not as a solar cell because the diffusion lengths were too short.

4.6. Other semiconductors

In one of their first papers on the SSPG method, Ritter and Weiser [3] also demonstrated its applicability to semi-insulating GaAs. Because of the longer diffusion length in this semiconductor, measurements at grating periods up to 70 µm were performed. The determined diffusion length was 10 µm, in agreement with alternative diffusion length measurements.

For high-band gap GaN and AlGaN/GaN double layers, Niehus and Schwarz [39,40] gave accounts on the application of SSPG. They report diffusion lengths up to 3 µm and find some relation between the Al doping and the excess carrier properties. The authors also raise some general questions concerning to applicability of SSPG and the meaning of the SSPG parameters in these experiments with high-band gap samples.

Thin-film chalcopyrite semiconductors were characterised soon after the SSPG method was proposed. Balberg *et al* [5] determined the majority and minority carrier properties of $CuGaSe_2$ thin films. The photo- to dark conductivity ratio was about 100 under their experimental conditions so that the experiments were not made impossible because of the background doping in these films. Here, electrons are the minority carriers for which the authors determined a diffusion length of 115 nm. From the intensity dependence of the mobility-lifetime products it was concluded that there is a sharp drop in the density-of-states in the band-gap close to the band edges – in contrast to a-Si:H.

Menner *et al* [41] report SSPG results on $CuGaSe_2$ thin films and determined the highest diffusion lengths for a Cu/Ga ratio at 0.95, i.e., close to the stochiometric point. SSPG-measurements in the Cu-rich region were impossible because of the high dark conductivity. Menner *et al* also aimed at revealing inhomogeneity in the growth process by application of a laser with a short absorption depth and by illumination from either the air/film and the substrate/film side. They concluded that a better crystal structure close to the substrate exists. These authors also raised the issue that transport may be different between in the direction of growth and perpendicular to it. A comparison with diffusion-length measurements in the direction of growth by spectral response suffered from the limited knowledge of the absorption coefficient of the CuGaSe films but indications were given that these diffusion lengths were a bit longer than those from SSPG.

Lubianiker *et al* [42] applied SSPG and photoconductivity for complementary measurements of $CuInS_2$ films. In this comprehensive study, the authors investigated both n-type and p-type samples by illumination from the air-side and the substrate-side. For the deduced recombination model and density-of-states distribution the reader is referred to the literature.

Belevich and Makovetskii [43] give an account of diffusion length measurements in polycrystalline p-type $CuInSe_2$. In their SSPG measurements in the range of grating periods of 4 µm to 9 µm with different electric field they determine photogeneration-rate dependent minority-electron diffusion lengths between 360 to 420 nm, decreasing with increasing photon flux. They relate the values of the diffusion length to the dimension of the crystallites in the polycrystalline film.

Generally, it is noted that one should not be too optimistic with respect to the application of SSPG to the $Cu(In,Ga)Se_2$ system. The experiment may be hampered by the large dark conductivity in $Cu(In,Ga)Se_2$, as was reported by Zweigart *et al* [44]. These authors have achieved to determine diffusion lengths for a variety of chemical compositions. But they also point out the difficulties in the SSPG application and evaluation. This is not surprising because the Fermi level is shifted towards the valence-band edge. If E_f is a few tens of meV above E_v the dark current will be too high. Higher photon flux for illumination may help or measuring at lower temperatures. Because the dark-current activation energy is also low, the decrease of the temperature will only help if the photocurrent does not decrease too much as well.

4.7. Further measurement modes

Schmidt and Longeaud [45] developed an analysis of the SSPG method with emphasis on the density-of-states determination at the quasi-Fermi energy. Several photocurrent measurements are needed at a specific grating period. From an RZW fit the additional parameter Z can be determined. From a variation of the temperature or the generation rate the quasi-Fermi energy can be shifted so that a scan can be performed. The application of the method was demonstrated on a-Si:H [45] and µc-Si:H [46]. In addition to the measurements performed in coplanar electrode configuration, other configurations have been studied. With respect to sandwich configurations, Bernhard *et al* [47] applied the SSPG method to amorphous semiconductor multilayer structures.

5. Summary

The evaluation of the experimental data on the basis of the RZW approach provides the basis of determining the ambipolar diffusion length in thin-film semiconductors when the experiment is performed under the necessary condition of small modulation depth, short enough dielectric relaxation time and sufficiently high photocurrent values with distinct differences between the minority-carrier and the majority-carrier mobility-lifetime product. A simple relationship between the diffusion length and the minority-carrier mobility-lifetime product can then be applied.

The overview over the range of applications introduced into the temperature, generation-rate and Fermi level dependence of the mobility-lifetime products in a-Si:H and other silicon-based thin-film semiconductors. Results on chalcopyrite and other semiconductors were briefly presented which show that SSPG can be a method of choice not only in thin-film silicon.

References

[1] Ritter D, Zeldov E and Weiser K 1986 Steady-state photocarrier grating technique for diffusion length measurement in photoconductive insulators *Applied Physics Letters* **49** 791

[2] Ritter D and Weiser K 1986 Ambipolar drift-length measurement in amorphous hydrogenated silicon using the steady-state photocarrier grating technique *Physical Review* B **34** 9031

[3] Ritter D, Weiser K and Zeldov E 1987 Steady-state photocarrier grating technique for diffusion-length measurement in semiconductors - theory and experimental results for amorphous-silicon and semiinsulating GaAs *Journal of Applied Physics* **62** 4563

[4] Bauer G H, Nebel C E, Mohring H-D 1988 Diffusion lengths in a-SiGe:H and a-SiC:H alloys from optical grating technique *Mater. Res. Soc. Symp. Proc.* **118** 679

[5] Balberg I, Albin D and Noufi R 1989 Mobility-lifetime products in $CuGaSe_2$ *Applied Physics Letters* **54** 1244

[6] Yang L, Catalano A, Arya R R and Balberg I 1990 Effect of low-level boron doping and its implication to the nature of gap states in hydrogenated amorphous-silicon *Applied Physics Letters* **57** 908

[7] Balberg I, Delahoy A E and Weakliem H A 1988 Self-consistency and self-sufficiency of the photocarrier grating technique *Applied Physics Letters* **53** 992

[8] Liu J Z, Li X, Roca i Cabarrocas P, Conde J P, Maruyama A, Park H and Wagner S 1990 Ambipolar diffusion length in a-Si-H(F) and a-Si,Ge-H,F measured with the steady-state photocarrier grating technique *Conf. record of the twenty first IEEE Photovoltaic Specialists Conf. (Kissimimee, USA, 21 – 25 May 1990)* (Piscataway: IEEE) p 1606

[9] Ritter D, Zeldov E and Weiser K 1988 Ambipolar transport in amorphous-semiconductors in the lifetime and relaxation-time regimes investigated by the steady-state photocarrier grating technique *Physical Review* B **38** 8296

[10] Balberg I 1990 The theory of the photoconductance under the presence of a small photocarrier grating *Journal of Applied Physics* **67** 6329

[11] Balberg I 1991 Theory of the small photocarrier grating under the application of an electric-field *Physical Review* B **44** 1628

[12] Li Y M 1990 Phototransport under the presence of a small steady-state photocarrier grating *Physical Review* B **42** 9025
[13] Sauvain E, Hubin J, Shah A and Pipoz P 1991 Effect of the dangling-bond charge on the ambipolar diffusion length in a-Si-H *Philosophical Magazine Letters* **63** 327
[14] Abel C-D, Bauer G H and Bloss W H 1995 Generalized theory for analytical simulation of the steady-state photocarrier grating technique *Philosophical Magazine* B **72** 551
[15] Hattori K, Okamoto H and Hamakawa Y 1992 Theory of the steady-state-photocarrier-grating technique for obtaining accurate diffusion-length measurements in amorphous-silicon *Physical Review* B **45** 1126
[16] Mohring H D and Abel C D, Brüggemann R and Bauer G H 1991 Characterization of high electronic quality a-SiC-H films by mu-tau products for electrons and holes *Journal of Non-Crystalline Solids* **137** 847
[17] Mohring H D, Abel C D, Brüggemann R and Bauer G H 1997 Characterization of high electronic quality a-SiC:H films by mu tau-products for electrons and holes *Journal of Non-Crystalline Solids* **210** 36 (Erratum to [16])
[18] Brüggemann R 1993 *PhD thesis* Philipps-Universität Marburg
[19] Brüggemann R, Abel C-D and Bauer G H 1992 Implications of the defect pool model for the simulation of a-Si:H solar cells *Proc. of the 11th E.C. Photovoltaics Solar Energy Conf. (Montreux, Switzerland, 12-16 October 1992)* ed L Guimaraes *et al* (Chur: Harwood Academic Publishers) p 676
[20] Brüggemann R and Badran R I 2004 Electric-field dependence of photocarrier properties in the steady-state photocarrier grating experiment *MRS Symp. Proc.* **808** 133
[21] Morgado E 2002 Light-soaking and annealing kinetics of majority and minority carrier mobility-lifetime products in a-Si:H *Journal of Non-Crystalline Solids* **299** 471
[22] Morgado E 2004 Influence of light-soaking and annealing on electron and hole mobility-lifetime products in a-Si:H *Journal of Non-Crystalline Solids* **338** 386
[23] Abel C D and Bauer G H 1993 Evaluation of the steady-state photocarrier grating technique with respect to a-Si:H and its application to a-SiGe:H alloys *Progress in Photovoltaics* **1** 269
[24] Fölsch J, Finger F, Kulessa T, Siebke F, Beyer W and Wagner H 1995 Improved ambipolar diffusion length in a-$Si_{1-x}Ge_x$:H alloys for multi-junction solar cells *MRS Symp. Proc.* **377** 517
[25] Gueunier M E, Kleider J P, Brüggemann R, Lebib S, Cabarrocas P R I, Meaudre R and Canut B 2002 Properties of polymorphous silicon-germanium alloys deposited under high hydrogen dilution and at high pressure *Journal of Applied Physics* **92** 4959
[26] Bhaduri A, Chaudhuri P, Williamson DL, Vignoli S, Ray P P and Longeaud C 2008 Structural and optoelectronic properties of silicon germanium alloy thin films deposited by pulsed radio frequency plasma enhanced chemical vapor deposition *Journal of Applied Physics* **104** 063709
[27] Li Y M, Fieselmann B F and Catalano A 1991 *Conf. Record 22nd IEEE Photovoltaic Specialists Conf. (Las Vegas, USA, 7 – 11 October 1991)* (Piscataway: IEEE) p 1231
[28] Droz C, Goerlitzer M, Wyrsch N and Shah, A 2000 Electronic transport in hydrogenated microcrystalline silicon: similarities with amorphous silicon *Journal of Non-Crystalline Solids* **266** 319
[29] Goerlitzer M, Beck N, Torres P, Meier J, Wyrsch N and Shah A 1996 Ambipolar diffusion length and photoconductivity measurements on ”midgap" hydrogenated microcrystalline silicon *Journal of Applied Physics* **80** 5111
[30] Brüggemann R 1998 Improved steady-state photocarrier grating in nanocrystalline thin films after surface-roughness reduction by mechanical polishing *Applied Physics Letters* **73** 499

[31] Okur S, Gunes M, Finger F and Carius R 2006 Diffusion length measurements of micro crystalline silicon thin films prepared by hot-wire/catalytic chemical vapor deposition (HWCVD) *Thin Solid Films* **501** 137
[32] Brüggemann R and Kunz O 2002 Temperature dependence of the minority-carrier mobility-lifetime product for probing band-tail states in microcrystalline silicon *Physica Status Solidi* B **234** R16
[33] Balberg I 2002 A simultaneous experimental determination of the distribution and character of the two band tails in disordered semiconductors *Journal of Optoelectronics and Advanced Materials* **4** 437
[34] Brüggemann R 2005 Mobility-lifetime products in microcrystalline silicon *Journal of Optoelectronics and Advanced Materials* **7** 495
[35] Brüggemann R, Brehme S, Kleider, J P, Gueuneier, M E and Bronner W 2004 Effects of proton irradiation on the photoelectronic properties of microcrystalline silicon *Journal of Non-crystalline Solids* **338-340** 77
[36] Günes M, Göktas O, Okur S, Isik N, Carius R, Klomfass J and Finger F 2005 Sub-bandgap absorption spectroscopy and minority carrier transport of hydrogenated microcrystalline silicon films *Journal of Optoelectronics and Advanced Materials* **7** 161
[37] Svrcek V, Fejfar A, Fojtik P, Mates T, Poruba A, Stuchlikova H, Pelant I, Kocka J, Nasuno Y, Kondo M and Matsuda A 2002 Importance of the transport isotropy in mu c-Si : H thin films for solar cells deposited at low substrate temperatures *Journal of Non-Crystalline Solids* **299** 395
[38] Badran R I, Brüggemann R and Carius R 2009 Minority-carrier properties of microcrystalline germanium *Journal of Optoelectronics and Advanced Materials* **11** 1464
[39] Niehus M and Schwarz R 2006 New results on diffusion lengths measurements in wide bandgap semiconductors, obtained from steady state photocarrier gratings (SSPG) *Superlattices and Microstructures* **40** 350
[40] Niehus M and Schwarz R 2006 Diffusion lengths in GaN obtained from steady state photocarrier gratings (SSPG) *Physica Status Solidi* C **3** 2103
[41] Menner R, Zweigart S, Klenk R and Schock H W 1993 Ambipolar diffusion length in $CuGaSe_2$ thin-films for solar-cell applications measured by steady-state photocarrier grating technique *Japanese Journal of Applied Physics* - Part 1 **32** 45
[42] Lubianiker Y, Biton G, Balberg I, Walter T, Schock H W, Resto O and Weisz SZ 1996 Dependence of the phototransport properties on the position of the Fermi level in polycrystalline $CuInS_2$ films *Journal of Applied Physics* **79** 876
[43] Belevich N N and Makovetskii G I 1994 Ambipolar diffusion and ambipolar carrier drift in $CuInSe_2$ films *Semiconductors* **28** 988
[44] Zweigart S, Menner R, Klenk R and Schock H W 1995 Application of the steady-state photocarrier grating technique for determination of ambipolar diffusion lengths in Cu(In,Ga)(S,Se)2-thin films for solar cells *Materials Science Forum* **173** 337
[45] Schmidt JA and Longeaud C 2005 Analysis of the steady-state photocarrier grating method for the determination of the density of states in semiconductors *Physical Review* B **71** 125208
[46] Souffi N, Bauer G H and Brüggemann R 2006 Density-of-states in microcrystalline silicon from thermally-stimulated conductivity *Journal of Non-Crystalline Solids* 352 1109
[47] Bernhard N and Bauer G H 1995 Physical-properties of a-Si:H based compositional periodic multilayers *Physical Review* B **52** 8829